RSC Advances

PAPER

View Article Online
View Journal | View Issue

Cite this: *RSC Adv.*, 2017, **7**, 51807

Zn_2GeO_4 nanorods grown on carbon cloth as high performance flexible lithium-ion battery anodes

T. T. Yu,[ab] H. L. Liu,[ab] M. Huang,[ab] J. H. Zhang,[*ab] D. Q. Su,[ab] Z. H. Tang,[ab] J. F. Xie,[ab] Y. J. Liu,[a] A. H. Yuan*[ab] and Q. H. Kong[c]

Received 22nd August 2017
Accepted 26th October 2017

DOI: 10.1039/c7ra09273c

rsc.li/rsc-advances

To improve the electrical conductivity and cycling stability of germanium compounds as anode materials for lithium ion batteries (LIBs), Zn_2GeO_4 nanorods grown on carbon cloth (Zn_2GeO_4/CC) were designed and fabricated by a simple hydrothermal process combined with a post-annealing treatment. The Zn_2GeO_4/CC composites possess hierarchical porosity and a network structure. Serving as free-standing and binder-free anodes for LIBs, they exhibit high specific capacity and excellent reversibility. A discharge capacity as high as 1851.9 mA h g^{-1} is attained at a current density of 200 mA g^{-1}, and the Zn_2GeO_4/CC electrode still maintains a high reversible capacity of 1302.3 mA h g^{-1} after 200 cycles. Even at a high specific current of 2000 mA g^{-1}, it still retains a capacity of 847.5 mA h g^{-1}. The superior electrochemical performance of the Zn_2GeO_4/CC composites is attributed to the synergistic effects of the hierarchical porosity, Zn_2GeO_4 nanorods, and 3D carbon cloth network structure, which can effectively accommodate the huge volume change of the Zn_2GeO_4 nanorods during cycling and maintain perfect electrical conductivity throughout the electrode. Moreover, the excellent mechanical flexibility of the Zn_2GeO_4/CC composites makes the material a promising candidate for self-supported and flexible electrodes for LIBs.

Introduction

Entering a new era of green energy, several criteria, such as cost, cycle life, safety, efficiency, energy, and power, need to be considered when developing electrical energy-storage systems for transportation and grid storage.[1–3] Rechargeable lithium ion batteries (LIBs) are one of the prospective candidates because of their inherent advantages including high energy density, long life span, no memory effect, and environmental nontoxicity.[4,5] However, although graphite used as an anode material in commercial LIBs offers stable cycling performance and low cost, its low theoretical capacity (372 mA h g^{-1}) greatly limits its further application in portable electronics and electric vehicles.

To date, many studies have been devoted to the development of high-capacity lithium alloying anodes of silicon (Si) and germanium (Ge) because of their high theoretical capacities of 4200 and 1600 mA h g^{-1}, respectively.[6–9] Between them, Ge has higher lithium-ion diffusivity than Si (400 times faster), higher electrical conductivity (104 times higher than that of Si), and low working potential. Nevertheless, the major drawbacks for the application of the pure Ge anode material are the high price and large volume expansion (370%) during the lithium alloying and dealloying processes, which lead to structural damage and rapid decay in the capacity, limiting the application of Ge anodes.[10] To reduce the price, germanium compounds, such as GeO_2 and Zn_2GeO_4, have been proposed as intriguing materials for lithium storage applications due to their high theoretical charge–discharge capacity.[11,12] GeO_2 can deliver a specific capacity of up to 2152 mA h g^{-1} and reversibly store 8.4 Li^+ ions, and Zn_2GeO_4 can also exhibit a high theoretical charge–discharge capacity of 1443 mA h g^{-1}.[13,14] Additionally, germanium compounds have several advantages over pure Ge, such as lower cost and better chemical stability and cyclability. Unfortunately, such binary or ternary Ge compounds are not effective for improving the cycling performance during drastic volume change and they have low electrical conductivity.

To address some of these issues related to the use of Ge and its compounds as anodes, many researchers have devoted attention to enhancing the electrochemical performances by constructing uniform hybrid structures with carbon, carbon nanotubes, graphene, *etc.* Paper-like free-standing Ge and single-walled carbon nanotube (SWCNT) composite anodes were prepared by the vacuum filtration of Ge/SWCNT composites. The paper anode with good Ge nanoparticle distribution in the SWCNT network offered better electrical contact, which aided the improvement of the capacity and cycling stability of the superior anodes in LIBs.[15] Mesoporous Ge/GeO_2/carbon

[a]*School of Environmental and Chemical Engineering, Jiangsu University of Science and Technology, Zhenjiang, Jiangsu 212003, China. E-mail: jhzhang6@just.edu.cn; aihua.yuan@just.edu.cn*

[b]*Marine Equipment and Technology Institute, Jiangsu University of Science and Technology, Zhenjiang, Jiangsu 212003, China*

[c]*School of the Environment and Safety Engineering, Jiangsu University, Zhenjiang, Jiangsu 212013, China*

composites were prepared by block copolymer directed coassembly, and exhibited high coulombic efficiency and reversible capacity (1631 mA h g^{-1}) and excellent cyclability due to the synergistic effects of the mesoporous structure, conductive carbon, and metallic Ge.[16] Co_2GeO_4/graphene nanocomposites were synthesized by a hydrothermal method, znd exhibited high reversible capacity and good cycling performance and rate capability due to the high electronic conductivity and high specific area of graphene.[17,18] In general, most carbon based composites employ either graphene or carbon nanotubes as the carbon substrates, and a traditional method needs to be used to further prepare electrodes with conductive carbon and a binder. This may cause some problems, such as the exfoliation of the active materials from the current collector, loss of the entire composite capacity, *etc.* If the active material can be directly coated onto some special substrate, a free-standing and binder-free electrode can be attained to overcome the disadvantages and achieve high performance.[19,20] Recently, Yu *et al.* fabricated a 3D hierarchical MoS_2 nanoflake array/carbon cloth with good rate discharging/charging stability as an anode material for flexible LIBs.[21]

In this work, a novel strategy was proposed for the simultaneous production of a high performance flexible Zn_2GeO_4/CC electrode. GeO_2 acted as a raw material because of the lower cost and an activated carbon fiber cloth was chosen as the conductivity framework for providing fast transport paths for electrons and lithium ions. Most importantly, Zn_2GeO_4/CC composites can be used directly as a free-standing and binder-free electrode. The hierarchical structure remains stable for Li^+ insertion and extraction and is hence expected to exhibit excellent charge–discharge performance. When evaluated as an anode material for LIBs, the as-formed Zn_2GeO_4/CC composites exhibited high reversible lithium storage capacity, long cyclability and excellent rate capability. The excellent electrochemical performance was attributed to the Zn_2GeO_4 nanorods, which were uniformly grown on the carbon cloth to form a porous surface structure and can provide a large electrode–electrolyte interfacial area, leading to an improved rate performance, and the porous Zn_2GeO_4/CC composites can buffer the large volume change caused in Zn_2GeO_4 during cycling. The developed strategy, being composed of a simple preparation method, using low-cost raw materials, and forming high-performance electrode products, will effectively promote the commercialization of flexible energy storage devices.

Experimental section

Materials

Zinc nitrate hexahydrate ($Zn(NO_3)_2 \cdot 6H_2O$, ≧99.0%), ammonium fluoride (NH_4F, ≧99.0%), urea ($CO(NH_2)_2$, ≧99.0%), and sodium hydroxide (NaOH, ≧99.0%) were purchased from the Aladdin Chemical Co. Germanium dioxide (GeO_2, ≧99.0%), nitric acid (HNO_3, ≧99.0%), ethanol, and acetone were obtained from the traditional Chinese Medicine Reagent Co. All the chemicals were used without further purification. Carbon cloth with hydrophilic surfaces (WOS 1002) was purchased from the Tianwan Carbon Technology Co.

Fabrication of Zn_2GeO_4/CC composites

The carbon cloth was cleaned by sonication sequentially in acetone, deionized water, and ethanol for 2 h, respectively. Subsequently, nitric acid was used to activate the well-cleaned carbon cloth for 6 h. The Zn_2GeO_4/CC composites were fabricated *via* a two-step process. In a typical process, 2 mmol $Zn(NO_3)_2 \cdot 6H_2O$, 1 mmol GeO_2, 2 mmol NH_4F, 5 mmol $CO(NH_2)_2$, and 4 mmol HNO_3 were dissolved in 30 mL of distilled water under continuous stirring. The pH value was adjusted to 8 by NaOH solution. Then, the homogeneous solution was transferred into Teflon-lined stainless autoclaves with carbon cloth (diameter of 13 mm) and heated at 200 °C for 24 h. After cooling down to room temperature, the products were collected and washed for at least three cycles using deionized water, and dried at 60 °C in a vacuum box. Afterwards, to improve the acting force between the Zn_2GeO_4 nanorods and carbon cloth, thermal treatment of the as-prepared product was performed at 450 °C for 2 h in N_2 atmosphere to obtain Zn_2GeO_4/CC composites. The mass loading of Zn_2GeO_4 on the carbon cloth was confirmed by weighing, and the results show that the average mass is about 16 mg on the carbon cloth (about 16 mg) with a diameter of 13 mm.

Structural characterization

The crystal structure and phase of the Zn_2GeO_4/CC composites were characterized by X-ray diffraction (XRD) measurements using a Shimadzu XRD-6000 diffractometer with Cu-Kα radiation (0.15406 nm). The surface electronic states were investigated by X-ray photoelectron spectroscopy (XPS, Thermo Fisher Scientific Escalab-250Xi using Al-Kα radiation) with a base pressure of 2×10^{-10} mbar. The surface morphology of the samples was depicted by field emission scanning electron microscopy (FESEM, ZEISS Merlin Compact). In addition, detailed microstructures were investigated using high resolution transmission electron microscopy (HRTEM, JEM-2100F) and energy dispersive X-ray spectroscopy (EDS, Oxford X-Max).

Electrochemical measurements

The Zn_2GeO_4/CC composites were used as working electrodes without adding any ancillary materials. Coin-type half cells (CR2032) were laboratory-assembled in an argon-filled glove box with the oxygen and water content below 1 ppm. A piece of the Zn_2GeO_4/CC composites was used directly as the working electrode. The non-aqueous electrolyte used in the cells was 1 mol L^{-1} $LiPF_6$ dissolved in ethylene carbonate and diethyl carbonate (EC : DEC, 1 : 1 in vol%). A Celgard 2400 microporous polypropylene membrane and Li foil were used as the separator and counter electrode, respectively. Coin-type half-cell charge and discharge tests were conducted on a LAND (China) battery program-control test system at various current densities between 0.01 and 3.0 V at 25 ± 1 °C. In this work, the capacity values were based on the mass of Zn_2GeO_4 and the carbon cloth acted as a support. The cyclic voltammetry (CV) curves were recorded on a CHI660D workstation (Shanghai, China) between 0.01 and 3 V (*vs.* Li^+/Li) at a scanning rate of 0.2 mV s^{-1}. The electrochemical impedance spectra (EIS) of the cells were also

recorded using the same instrument by applying a sine wave with an amplitude of 70 mV at a frequency range from 100 kHz to 0.01 Hz.

Results and discussion

The synthesis strategy of the Zn_2GeO_4/CC electrode is schematically illustrated in Fig. 1, where Zn_2GeO_4 nanorods are grown on the surface of a carbon fibre cloth. The surface changes from smooth to porous because of the anisotropic growth of the Zn_2GeO_4 nanorods. The interlaced network porous structure of the carbon cloth is favorable for the electrochemical reaction of the lithium ions. The formation of Zn_2GeO_4 nanorods can effectively accommodate the huge volume change. The FESEM images in Fig. 2 show the morphologies of the carbon cloth, commercial GeO_2, and Zn_2GeO_4/CC composites. In the images in Fig. 2a, the carbon cloth shows a microstructure of compact bundle fibers, which is actually an artificial pseudo-two-dimensional network with an ordered texture structure, and each carbon fiber with a smooth surface has a uniform diameter of around 8.5 μm. Fig. 2b shows that the commercial GeO_2 samples are bulky grains with diameters of more than 5 μm. It is well known that the large volume expansion of anode materials will lead to a rapid decline in the capacity during the lithiation and delithiation processes. Therefore, to decrease the size, enhance the conductivity, and reduce the cost, Zn_2GeO_4/CC composites were devised and fabricated using commercial GeO_2 grains as raw materials and carbon cloth as a conductivity network structure, respectively. Fig. 2c is a FESEM image of the Zn_2GeO_4/CC composites showing that the fiber structure of the carbon cloth still remained. The carbon fiber is covered with numerous Zn_2GeO_4 nanorods, and the Zn_2GeO_4/CC composite fibers have a uniform diameter of approximately 10 μm. The high magnification image in Fig. 2d shows that the Zn_2GeO_4 nanorods have uniform size with a length and diameter of about 80 nm and 30 nm, respectively. The mass ratio of the Zn_2GeO_4 nanorods to carbon cloth is about 1 : 1, which was confirmed by weighing. The composites create a hierarchical nanostructure with abundant open space and an electroactive surface and buffer the volume change resulting from external bending and repeated Li^+ insertion–extraction. Additionally, the carbon cloth is a highly conductive textile with excellent mechanical flexibility and strength.

The crystal structure and composition of the Zn_2GeO_4 nanorods were further analyzed by TEM, HRTEM and EDS, and

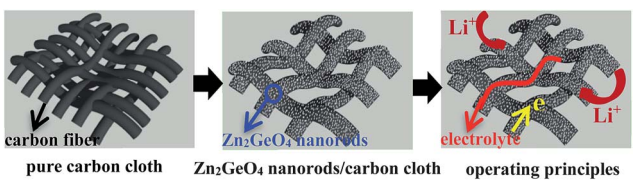

Fig. 1 A schematic illustration of the synthesis of flexible 3D Zn_2GeO_4 nanorods/carbon cloth and the operating principles when used in rechargeable LIBs.

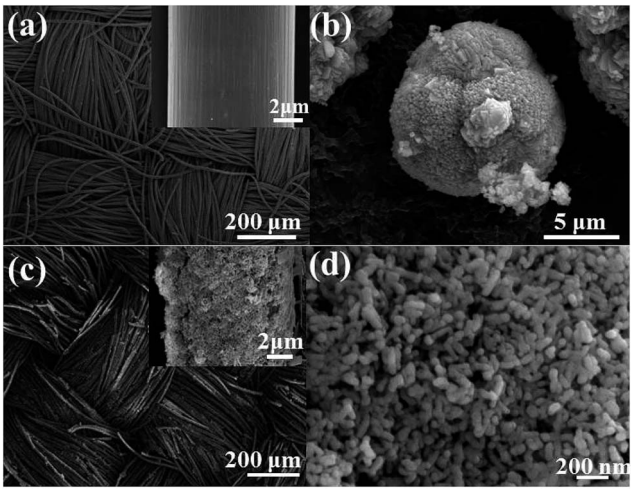

Fig. 2 (a) The FESEM image of pure carbon cloth, and the inset is the FESEM image of a single carbon fiber; (b) the commercial GeO_2 powder; (c and d) the Zn_2GeO_4/CC composites with different magnifications, and the inset in (c) is the FESEM image of a single Zn_2GeO_4/CC fiber.

the Zn_2GeO_4 nanorods were obtained by the sonication of the Zn_2GeO_4/CC composites in an *N*-methyl pyrrolidone solvent. Fig. 3a is a low magnification TEM image of the Zn_2GeO_4 nanorods, which shows that the size of the Zn_2GeO_4 nanorods is relatively uniform. Fig. 3b shows the high magnification TEM image of a single Zn_2GeO_4 nanorod, revealing that the diameter is about 30 nm. Fig. 3c is the HRTEM image of a Zn_2GeO_4 nanorod, and the inset is its corresponding selected area electron diffraction (SAED) image, revealing that a Zn_2GeO_4 nanorod is perfectly monocrystalline. The well-defined lattice fringes with lattice spacings of 0.71 nm and 0.30 nm correspond to the (110) and (113) lattice planes of the rhombohedral phase of Zn_2GeO_4, respectively. This suggests that the growth direction of the Zn_2GeO_4 nanorods was along the [110] plane.[22] Furthermore, the combination of the EDS spectrum with the element mapping images of Zn_2GeO_4 provides evidence for the existence of a homogeneous distribution of Zn, Ge and O elements, as shown in Fig. 3d and e. Fig. 3f shows the images of the 3D interconnected Zn_2GeO_4/CC electrode, which can be easily curved with tweezers. It can be clearly observed that the electrodes exhibited excellent flexibility, which makes them possible for application in flexible devices.

The composition and phase purity of the carbon cloth and Zn_2GeO_4/CC composites were examined by XRD and are represented in Fig. 4. The sharp and strong diffraction peaks can be indexed to rhombohedral Zn_2GeO_4 (JCPDS card no. 011-0687) with lattice constants of $a = b = 1.4231$ nm and $c = 0.953$ nm.[23] The observed peaks at 26° and 43° can be ascribed to the (002) and (101) planes of the carbon cloth substrate, which can also be observed in the XRD pattern of the pure carbon cloth. No additional diffraction peaks other than those of Zn_2GeO_4 and the carbon cloth were observed, implying the high purity of the Zn_2GeO_4/CC composites. To gain further insight into the chemical composition of the Zn_2GeO_4 nanorods, XPS measurement was performed. As shown in Fig. 5a, the survey

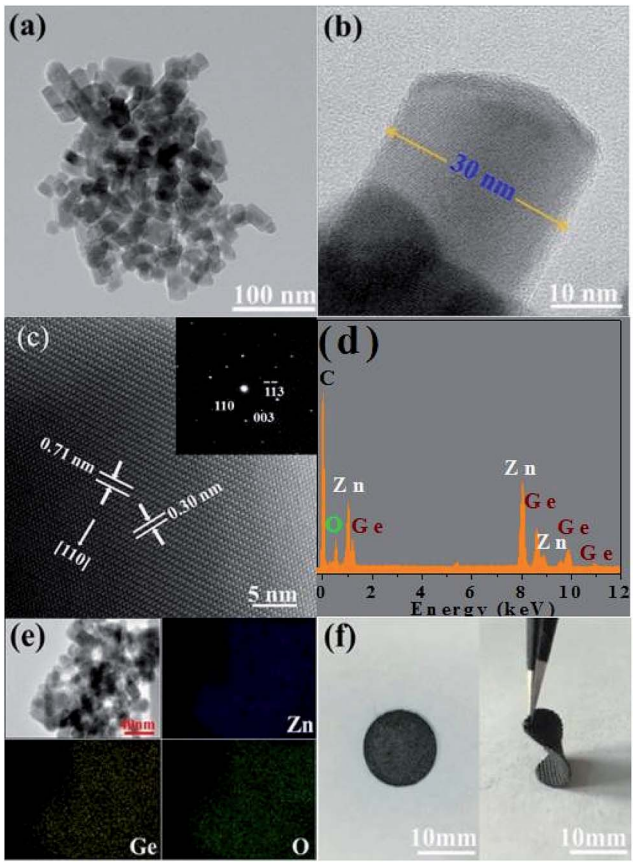

Fig. 3 (a) A TEM image of the Zn_2GeO_4 nanorods; (b) a TEM image of a single Zn_2GeO_4 nanorod; (c) a HRTEM image of a Zn_2GeO_4 nanorod, and the inset is a SAED image; (d) an EDS of the Zn_2GeO_4 nanorods; (e) a TEM image of the Zn_2GeO_4 nanorods and corresponding elemental mapping of Zn, Ge, and O; (f) the photographs of the prepared electrode.

XPS spectrum revealed that the sample was composed of Zn, Ge and O species. Fig. 5b shows a high-resolution Zn 2p XPS spectrum, which shows two typical characteristic peaks of the oxidation state of Zn^{2+}, corresponding to Zn $2p_{3/2}$ and Zn $2p_{1/2}$

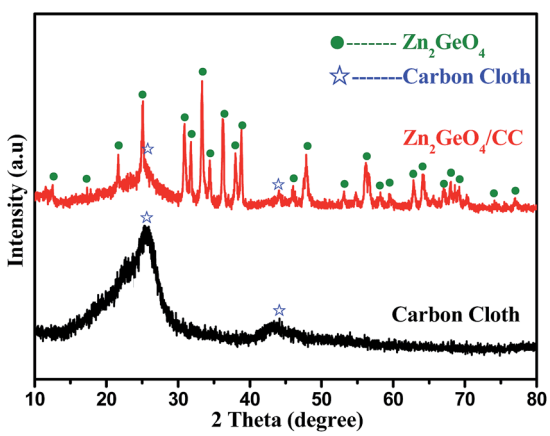

Fig. 4 The XRD patterns of the carbon cloth and Zn_2GeO_4/CC composites.

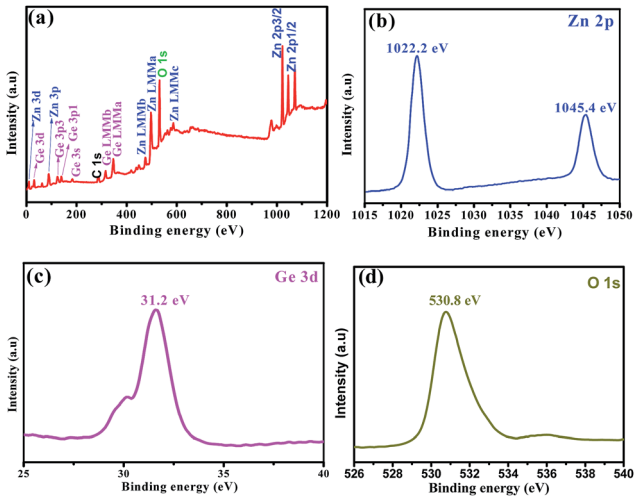

Fig. 5 The XPS spectra of the Zn_2GeO_4 nanorods: (a) a survey scan spectrum; (b) the Zn 2p spectrum; (c) the Ge 3d spectrum; (d) the O 1s spectrum.

at 1022.18 eV and 1045.4 eV. The high-resolution Ge 3d XPS spectrum (Fig. 5c) presents a sharp peak at 31.2 eV, which could be attributed to the Ge–O bond. Finally, the observed peak at 530.81 eV is assigned to O 1s, as shown in Fig. 5d.

To evaluate the electrochemical lithium storage of the unique microstructure, the 3D porous Zn_2GeO_4/CC composites were directly applied as anodes for LIBs. Fig. 6a shows the first three CV curves of the Zn_2GeO_4/CC electrode in the voltage range of 0–3 V at a scan rate of 0.1 mV s^{-1}. During the initial cathodic sweep, a strong reduction peak at around 0.28 V was observed, which was assigned to the decomposition of Zn_2GeO_4 as well as irreversible reactions that are related to the formation of SEI films and the decomposition of the electrolyte. This peak

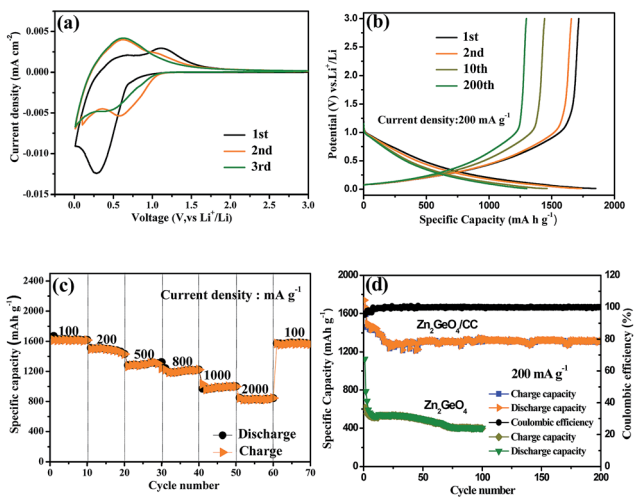

Fig. 6 The electrochemical performances of Zn_2GeO_4/CC as anode materials for LIBs: (a) the CV curves; (b) the charge–discharge curves at a current density of 200 mA g^{-1}; (c) the capacity *versus* the cycle number plot at different charging rates; (d) the continued cycling performance.

shifts to 0.58 V in the second cycle and 0.43 V in the third cycle. The irreversible phenomenon in the first several cycles was partially attributed to the multistep reaction of Zn_2GeO_4. In the anodic scan process, a broad oxidation peak at 1.1 V was observed, which was associated with the delithiation of the Li-metal alloys. Remarkably, the CV curves did not change significantly after the first cycle, revealing good stability and reversibility for the insertion and exaction of lithium ions. Fig. 6b presents the voltage–capacity profiles of the Zn_2GeO_4/CC anode for the 1st, 2nd, 10th, and 200th cycles at a current rate of 200 mA g^{-1} between 0.01 and 3.0 V. During the first discharge process, the main potential plateau is located at around 0.1 V (*vs.* Li^+/Li), which agrees well with the lithiation process of Zn_2GeO_4, and the initial discharge/charge capacity is found to be 1851.9/1716.2 mA h g^{-1}, corresponding to the initial coulombic efficiency (CE) of 92.7%. In general, the irreversible capacity loss is mainly attributed to the formation of a solid electrolyte interface (SEI) membrane from the decomposition of the electrolyte, which is commonly observed for most anode materials.[24,25] The Zn_2GeO_4/CC composites exhibited sloping voltage profiles, and the long plateaus at about 0.74 V shown in the first discharge disappeared during the 2nd, 10th, and 200th discharges, suggesting that the reductive decomposition of the electrolyte was effectively prevented due to the formation of a SEI film in the first discharge, which greatly relieved the irreversible capacity loss of the following cycles.[26,27] Therefore, the second discharge/charge capacity is found to be 1659.5/1595.8 mA h g^{-1}, and the CE increases to 96.1%. After the 200th cycle, the reversible capacity maintained a nearly constant value of approximately 1302.3 mA h g^{-1} and the CE steadily reached about 99.9%.

The rate performance of the Zn_2GeO_4/CC electrode was further studied by cycling at different current densities ranging from 100 to 2000 mA g^{-1}. As shown in Fig. 6c, the capacity decreased from 1615.9 to 1496, 1265.8, 1222.2, 1032.1 and 847.5 mA h g^{-1} when the current density was increased from 100 to 200, 500, 800, 1000, and 2000 mA g^{-1}, respectively. Notably, a capacity of 847.5 mA h g^{-1} was retained at the relatively high current density of 2000 mA g^{-1}, illustrating the high rate capability of the Zn_2GeO_4/CC electrode. After cycling at the highest current density of 2000 mA g^{-1}, the capacity recovered to about 1573.4 mA h g^{-1} as the current density was switched back to 100 mA g^{-1}, corresponding to a capacity retention of ~97.4%, which indicates high stability as well as excellent reversibility of the electrode. Fig. 6d displays the cycling performance and coulombic efficiency of the Zn_2GeO_4/CC electrode at 200 mA g^{-1} for 200 cycles in a voltage range of 0.01 to 3 V. After 200 cycles, the anode still had a reversible discharge capacity of 1302.3 mA h g^{-1}, reaching 50.6% of the first discharge capacity. Meanwhile, the CE quickly increased to 92.7% for the second cycle from 68.6% for the first cycle, and furthermore, it approached 99.9% after 200 cycles, showing excellent reversibility of the electrode. For comparison, the Zn_2GeO_4 nanorods were also selected to do comparative experiments by the same assembly process, and the capacity profile for 100 charge–discharge cycles is shown in Fig. 6d. The reversible capacities of the Zn_2GeO_4 nanorods can be retained at 398 mA h g^{-1} at the end of 100 charge–discharge cycles, and they also present decent cyclic stability. Nevertheless, the reversible capacity of the Zn_2GeO_4 nanorods is lower than that of the Zn_2GeO_4/CC composites. The improved rate performance was attributed to the Zn_2GeO_4/CC electrode buffering the large volume change, and the hierarchical structure remained stable for Li-ion insertion and extraction.

To further understand the lithium-storage properties, an AC impedance measurement was employed. The electrochemical impedance spectra (EIS) of the Zn_2GeO_4/CC composites were investigated with a fresh cell and after 200 cycles at 200 mA g^{-1}, as shown in Fig. 7. The Nyquist plots consist of one semicircle in the high frequency region and a straight line in the low frequency region. The semicircle portion is related to the reactions occurring on the electrode–electrolyte interface, which reflects the charge transfer impedance and SEI impedance. The results show that the Zn_2GeO_4/CC composite electrode after 200 cycles exhibited lower charge transfer resistance than the fresh cell, which indicates that the fresh cell had the highest charge transfer resistance. Compared with the inset, the semi-circle of the Zn_2GeO_4/CC electrode at high frequency is much smaller than that of the carbon cloth, indicating that the Zn_2GeO_4/CC electrode also had lower charge transfer resistance than the carbon cloth. This decreased charge transfer resistance was attributed to the improved electrical contact between the Zn_2GeO_4 nanorods and carbon cloth substrate.[28,29] The whole impedance value of the Zn_2GeO_4/CC electrode decreased when undergoing cycling, implying a better electrochemical performance based on the knowledge of traditional planar electrodes.[30] However, the Zn_2GeO_4/CC electrode suffered an obvious capacity decay, which can be interpreted as a small part of the Zn_2GeO_4 nanorods detaching from the carbon cloth after 200 cycles, resulting in the decreased capacity.[31] Additionally, the results suggest that the higher diffusivity of the lithium ions with the increasing charge–discharge cycles reduced the charge transfer resistance. To confirm the 3D porous Zn_2GeO_4/CC network structure can relieve the volume expansion, the morphology and structure of the Zn_2GeO_4/CC electrode after 20 cycles at 200 mA g^{-1} were characterized by FESEM observations.

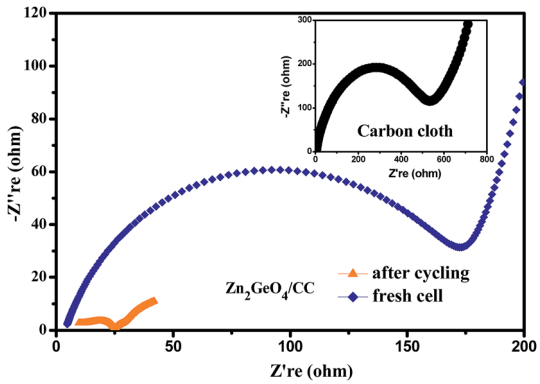

Fig. 7 The Nyquist plots of the Zn_2GeO_4/CC electrode with a fresh cell and after the 200th cycle at 200 mA g^{-1}, and the inset is the Nyquist plot of the pure carbon cloth.

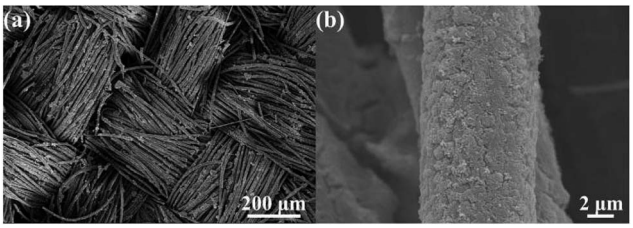

Fig. 8 The FESEM images of the Zn_2GeO_4/CC electrode were observed after 10 charge/discharge cycles at 200 mA g^{-1}.

Fig. 8 clearly shows that the Zn_2GeO_4/CC composite anode retains its initial appearance after the cycling test, indicating good stability of the Zn_2GeO_4/CC composite during the process of Li^+ charge/discharge.

The high reversible capacity and excellent cyclic stability and rate capability were attributed to the novel 3D network structure of the Zn_2GeO_4/CC electrode. First, the Zn_2GeO_4 nanorods guaranteed fast Li-ion diffusion, while the thin and porous surface structure of Zn_2GeO_4 on the carbon cloth improved electrolyte penetration and further facilitated the Li-ion transport, thus contributing to the significant improvement in the cycling performance.[32,33] Secondly, the soft and flexible carbon cloth buffered the volume expansion of Zn_2GeO_4, while the interconnected carbon fibers served as channels for electron transport.[34,35] Thirdly, the synergistic effect between the Zn_2GeO_4 nanorods and carbon cloth was of great importance. The 3D hierarchical structures of the Zn_2GeO_4/CC electrode provide a large surface area for active material loading while maintaining a shorter Li ion diffusion distance, leading to a high reversible capacity. The loose textures and open spaces between the neighboring fibers facilitated electrolyte diffusion and the accommodation of strain induced by the volume change during the Li ion insertion/extraction process.[36–38] Therefore, such a novel Zn_2GeO_4/CC electrode exhibited high reversible capacity and excellent cyclic stability and rate capability.

Conclusions

In summary, Zn_2GeO_4/CC composites have been successfully fabricated *via* a simple hydrothermal method combined with a post-annealing treatment. The well-defined porous 3D Zn_2GeO_4/CC composites were obtained with uniform coating of the Zn_2GeO_4 nanorods on the carbon cloth, and the Zn_2GeO_4 nanorods have uniform and small size. When evaluated as an anode material for LIBs, the porous Zn_2GeO_4/CC composites exhibit enhanced reversible capacity of 1302.3 mA h g^{-1} at 200 mA g^{-1} after 200 cycles. Even at high specific currents of 2000 mA g^{-1}, they still retained a capacity of 847.5 mA h g^{-1}. The excellent cycling stabilities and rate capabilities are attributed to the small size of the Zn_2GeO_4 nanorods, small volume expansion due to the thin and porous surface structure of Zn_2GeO_4 on the carbon cloth, and high conductivity of the carbon cloth with a network structure. The approach is generic and can be applied using cheap sources to obtain high-performance, and highly valuable porous carbon cloth based composites are expected to promote the practical application of wearable and portable energy storage devices.

Conflicts of interest

There are no conflicts to declare.

Acknowledgements

The work was financially supported by the Natural Science of Foundation of China (No. 51672114, 51603091), Natural Science Foundation of Jiangsu Province (No. BK 20150505), Open Project Program of Key Laboratory of Eco-textiles, Ministry of Education, Jiangnan University (No. KLET1609), China Postdoctoral Science Foundation (No. 2017M611747), Foundation for Marine Equipment and Technology Institute for Jiangsu University of Science and Technology (No. HZ20170015), and Qinglan Project of Jiangsu Province (No. 1114901602).

Notes and references

1 J. F. Cui, Y. L. Xi, S. Chen, D. H. Li, X. L. She, J. Sun, W. Han, D. J. Yang and S. J. Guo, *Adv. Funct. Mater.*, 2016, **26**, 8487–8495.
2 D. Ji, H. Zhou, Y. L. Tong, J. P. Wang, M. Z. Zhu, T. H. Chen and A. H. Yuan, *Chem. Eng. J.*, 2017, **313**, 1623–1632.
3 Y. Jiang, Y. Z. Feng, B. J. Xi, S. S. Kai, K. Mi, J. K. Feng, J. H. Zhang and S. L. Xiong, *J. Mater. Chem. A*, 2016, **4**, 10719–10726.
4 K. S. Chen, R. Xu, N. S Luu, E. B. Secor, K. Hamamoto, Q. Q. Li, S. Kim, V. K. Sangwan, I. Balla, L. M. Guiney, J. W. T. Seo, X. K. Yu, W. W. Liu, J. S. Wu, C. Wolverton, V. P. Dravid, S. A. Barnett, J. Lu, K. Amine and M. C. Hersam, *Nano Lett.*, 2017, **17**, 2539–2546.
5 A. Paolella, C. Faure, G. Bertoni, S. Marras, A. Guerfi, A. Darwiche, P. Hovington, B. Commarieu, Z. R. Wang, M. Prato, M. Colombo, S. Monaco, W. Zhu, Z. M. Feng, A. Vijh, C. George, G. P. Demopoulos, M. Armand and K. Zaghib, *Nat. Commun.*, 2017, **8**, 14643.
6 X. X. Zuo, J. Zhu, P. Mueller-Buschbaum and Y. J. Cheng, *Nano Energy*, 2016, **31**, 113–143.
7 N. Lin, Y. Han, J. Zhou, K. L. Zhang, T. J. Xu, Y. C. Zhu and Y. T. Qian, *Energy Environ. Sci.*, 2015, **8**, 3187–3191.
8 T. Kennedy, M. Brandon and K. M. Ryan, *Adv. Mater.*, 2016, **28**, 5696–5704.
9 S. Choi, Y. G. Cho, J. Kim, N. S. Choi, H. K. Song, G. X. Wang and S. Park, *Small*, 2017, **13**, 1603045.
10 C. Zhong, J. Z. Wang, X. W. Gao, D. Wexler and H. K. Liu, *J. Mater. Chem. A*, 2013, **1**, 10798–10804.
11 W. Wang, J. Qin and M. Cao, *ACS Appl. Mater. Interfaces*, 2016, **8**, 1388–1397.
12 J. H. Zhang, T. T. Yu, J. L. Chen, H. L. Liu, D. Q. Su, Z. H. Tang, J. F. Xie, L. Chen, A. H. Yuan and Q. H. Kong, *Ceram. Int.*, 2017, **44**, 1127–1133.
13 Y. Chen, C. L. Yan and O. G. Schmidt, *Adv. Energy Mater.*, 2013, **3**, 1269–1274.

14 C. Wang, W. Wan, Y. H. Huang, J. T. Chen, H. H. Zhou and X. X. Zhang, *Nanoscale*, 2014, **6**, 5351–5358.
15 J. Wang, J. Z. Wang, Z. Q. Sun, X. W. Gao, C. Zhong, S. L. Chou and H. K. Liu, *J. Mater. Chem. A*, 2014, **2**, 4613–4618.
16 J. Hwang, C. Jo, M. G. Kim, J. Y. Chun, E. Lim, S. Kim, S. Jeong, Y. Kim and J. Lee, *ACS Nano*, 2015, **9**, 5299–5309.
17 F. Zhang, R. H. Zhang, Z. Zhang, H. K. Wang, J. K. Feng, S. L. Xiong and Y. T. Qian, *Electrochim. Acta*, 2014, **150**, 211–217.
18 H. L. Liu, T. T. Yu, D. Q. Su, Z. H. Tang, J. H. Zhang, Y. J. Liu, A. H. Yuan and Q. H. Kong, *Ceram. Int.*, 2017, **43**, 14395–14400.
19 G. H. Zhang, S. C. Hou, H. Zhang, W. Zeng, F. L. Yan, C. C. Li and H. G. Duan, *Adv. Mater.*, 2015, **27**, 2400–2405.
20 D. Ji, H. Zhou, Y. Y. Dan, H. X. Yang and A. H. Yuan, *J. Mater. Chem. A*, 2016, **4**, 8283–8290.
21 H. L. Yu, C. L. Zhu, K. Zhang, Y. J. Chen, C. Y. Li, P. Gao, P. P. Yang and Q. Y. Ouyang, *J. Mater. Chem. A*, 2014, **2**, 4551–4557.
22 J. Liang, Y. Q. Cao, H. Lin, Z. Z. Zhang, C. C. Huang and X. X. Wang, *Inorg. Chem.*, 2013, **52**, 6916–6922.
23 W. Liu, T. F. Zhou, Y. Zheng, J. W. Liu, C. Q. Feng, Y. Shen, Y. H. Huang and Z. P. Guo, *ACS Appl. Mater. Interfaces*, 2017, **9**, 9778–9784.
24 M. Huang, K. Mi, J. H. Zhang, H. L. Liu, T. T. Yu, A. H. Yuan, Q. H. Kong and S. L. Xiong, *J. Mater. Chem. A*, 2017, **5**, 266–274.
25 Y. L. Tong, D. Ji, P. Wang, H. Zhou, K. Akhtar, X. P. Shen, J. H. Zhang and A. H. Yuan, *RSC Adv.*, 2017, **7**, 25182–25190.
26 T. S. Sahu and S. Mitra, *Sci. Rep.*, 2015, **5**, 12571.
27 J. Zhang, Z. X. Yang, J. Qiu and H. W. Lee, *J. Mater. Chem. A*, 2016, **4**, 5802–5809.
28 J. H. Zhang, M. Huang, B. J. Xi, K. Mi, A. H. Yuan and S. L. Xiong, *Adv. Energy Mater.*, 2017, DOI: 10.1002/aenm.201701330.
29 Y. S. Su and A. Manthiram, *Nat. Commun.*, 2012, **3**, 1166.
30 J. Guo, A. Sun, X. Chen, C. Wang and A. Manivannan, *Electrochim. Acta*, 2011, **56**, 3981–3987.
31 W. Weng, Q. Q. Wu, Q. Sun, X. Fang, G. Z. Guan, J. Ren, Y. Zhang and H. S. Peng, *J. Mater. Chem. A.*, 2015, **3**, 10942–10948.
32 F. Mattelaer, K. Geryl, G. Rampelberg, J. Dendooven and C. Detavernier, *ACS Appl. Mater. Interfaces*, 2017, **9**, 13121–13131.
33 H. C. Shim, I. Kim, C. S. Woo, H. J. Lee and S. Hyun, *Nanoscale*, 2017, **9**, 4713–4720.
34 M. S. Balogun, W. T. Qiu, F. Y. Lyu, Y. Luo, H. Meng, J. T. Li, W. J. Mai, L. Q. Mai and Y. X. Tong, *Nano Energy*, 2016, **26**, 446–455.
35 L. B. Dong, C. J. Xu, Y. Li, Z. Z. Pan, G. M. Liang, E. L. Zhou, F. Y. Kang and Q. H. Yang, *Adv. Mater.*, 2016, **28**, 9313–9319.
36 B. Liu, J. Zhang, X. F. Wang, G. Chen, D. Chen, C. W. Zhou and G. Z. Shen, *Nano Lett.*, 2012, **12**, 3005–3011.
37 J. H. Zhang, S. Wan, B. Yan, L. B. Wang and Y. T. Qian, *J. Nanosci. Nanotechnol.*, 2013, **13**, 4364–4369.
38 G. H. Zhang, S. C. Hou, H. Zhang, W. Zeng, F. L. Yan, C. Chao and H. G. Duan, *Adv. Mater.*, 2015, **27**, 2400–2405.